FREE-VORTEX FLOW SIMULATION USING A THREE-DIMENSIONAL EULER AERODYNAMIC METHOD

ICAS-86-1.5.2

P. Raj, J.S. Sikora, and J.M. Keen
Lockheed-California Company
Burbank, California, U. S. A.

Abstract

A computational method based on a finite-volume, multistage Runge-Kutta pseudo-time-stepping algorithm to solve the three-dimensional Euler equations is used to simulate free vortices generated by separation of flow along the edges of swept, slender wings at moderate-to-high angles of attack. The flow is impulsively started and the vortices are automatically captured. Two issues are specifically addressed: (1) Sensitivity of the solutions to artificial viscosity, and (2) Effect of grid density on the results. Computed results for a cropped-delta wing, an arrow wing, and a strake-wing-body configuration are correlated with experimental data and, wherever possible, with predictions of other numerical methods. Relatively small changes in the subsonic solutions are noticed with variations in the magnitude of artificial viscosity and grid density, as long as the free vortices are generated along sharp edges. The correlations presented here provide an added measure of confidence in computational simulations using the Euler equations. The present investigation also raises some new issues related to vortex instabilities.

Introduction

The accurate computational simulation of three-dimensional flows dominated by the interaction of free vortices with lifting surfaces is of considerable interest to aircraft designers. This problem is of special significance for supersonic-cruise aircraft which have highly swept slender wings for desirable performance in cruise. During low-speed flight and transonic maneuvering at moderate-to-high angles of attack, the flow invariably separates from the leading edges resulting in the formation of free vortices above the wing. Significant improvements in aerodynamic performance can be derived by careful generation and control of these vortices, as illustrated in Figure 1. At present, a designer has to rely on extensive and costly wind-tunnel tests for necessary data. Accurate, efficient, and reliable computational methods for free-vortex flow simulation are needed to complement the experimental tests. It is important to note that the ability to model the nonlinear aerodynamics of the configurations exhibiting free-vortex flows is a crucial requirement for these methods.

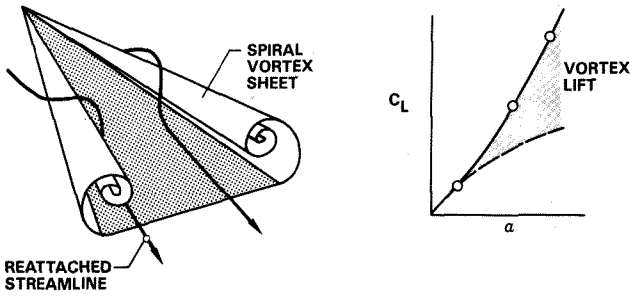

Figure 1. Benefits of Vortex Flow for Slender Swept Wings

Research on free-vortex flow simulation has produced a number of computational methods. At one end of the spectrum are the vortex-lattice [1-4] and free-vortex-sheet (FVS) methods [5,6]. Since they are based on a linearized potential-flow formulation, the vortices have to be explicitly modeled either indirectly, using the suction analogy of Polhamus [7] or directly using singularity distributions [4,5]. For the latter, the location and shape of the vortices have to be determined iteratively, since the rotational flows cannot evolve as a part of the solution of a potential flow code. At the other end of the spectrum are field methods based on Reynolds-averaged Navier-Stokes equations [8], which provide an essentially complete fluid-dynamic model. Their use offers a major advantage in that the leading-edge vortices evolve naturally as a part of the solution. However, the available methods are not suitable for routine practical applications due to the exorbitant requirements of computational resources and the lack of a suitable universal turbulence model. Ongoing developments of supercomputers and research in turbulent flow simulations promise to overcome these obstacles in the coming years.

Recent advances in numerical algorithms to solve the Euler equations [9,10] provide an attractive and cost-effective alternative to using Navier-Stokes codes. Their ability to automatically capture regions of rotational flows has been demonstrated in several investigations [11-15]. In this paper, results for a cropped-delta wing, an arrow wing, and a strake-wing-body configuration are presented that specifically

address two critical issues related to the use of the Euler codes: (1) Sensitivity of the solution to artificial viscosity; and (2) Effect of grid density on the results.

A Three-dimensional Euler Aerodynamic Method, TEAM, is used in the present investigation. Its algorithm is briefly outlined in the next section, followed by correlation of computed results with experimental data in the Results & Discussion section.

Three-dimensional Euler Aerodynamic Method

The explicit pseudo-time-stepping, finite-volume algorithm of Jameson et al. [9] forms the core of the TEAM code. Only the basic features are highlighted in this section. Additional details can be found in References 9, 10, 12, 14, 16, and 17.

In this algorithm, the region surrounding a given configuration is subdivided into small hexahedral cells. These cells may, in principle, be constructed in any convenient manner; only the Cartesian coordinates on the cell vertices are required. The version of the code used in this investigation can accommodate cells arranged according to boundary-conforming C-H, C-O, O-O, or O-H topologies. The C-H topology is illustrated in Figure 2; others may be analogously defined.

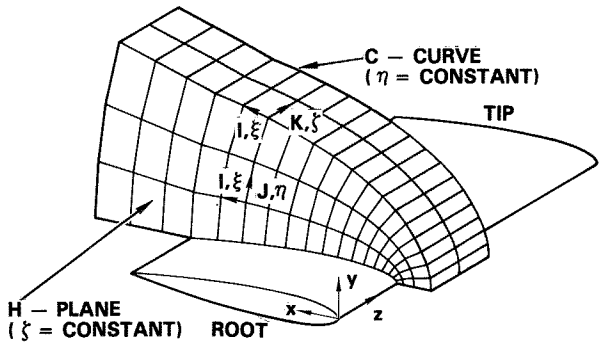

Figure 2. C-H Topology

In each of the cells, the semi-discrete approximations to the time-dependent Euler equations, representing mass, momentum, and energy conservation, are integrated using a multistage Runge-Kutta scheme. Convergence to steady state is typically achieved in a few hundred time steps, since the step size for each cell is determined by local stability restrictions. In contrast, thousands of steps are required when using a conventional explicit scheme with a global minimum-step size. Enthalpy damping and implicit residual smoothing further reduce the number of time steps required to reach the steady state. Appropriate nonreflecting boundary conditions are used at the far-field boundaries. A no-normal-flow condition is imposed on the solid surface.

The finite-volume spatial discretization reduces to a central-difference scheme which is formally second-order accurate for smooth grids. This scheme is augmented by adaptive dissipation terms (also known as artificial or numerical viscosity) in order to suppress its well-known tendency for odd-even point decoupling, to capture shocks automatically, and to minimize pre- and post-shock oscillations. The dissipation terms, composed of second and fourth differences, are constructed such that their values are small compared to those of the convective terms, except in some isolated regions. Therefore, possible contamination of an inviscid solution of the Euler equations is localized.

The user-specified coefficient (VIS-2) of the second-difference terms is scaled by the second derivative of static pressure. This introduces a larger amount of dissipation where it is needed the most -- near shocks and stagnation points -- to suppress wiggles and overshoots. Elsewhere, their contribution is small. The fourth-difference terms are scaled by a user-input coefficient, VIS-4, divided by 64. Similar scalings have been used by other investigators [9,17]. These terms provide the necessary background dissipation to suppress the high-frequency error components and thereby minimize aliasing errors. They are turned off in regions where their values are smaller than those of the second-order terms. The input values of VIS-2 and VIS-4 are typically of order one. Their effect on the solution is discussed in the following section.

Results & Discussion

In this section, corrrelations of results computed using the TEAM code with experimental data are presented for three cases: a cropped-delta wing, an arrow wing, and a strake-wing-body configuration. For each case, the entire domain is initialized to free-stream conditions. This is equivalent to impulsively starting the configuration. No Kutta condition is explicitly applied. A brief discussion of the role of numerical dissipation in generating the free vortices follows the presentation of the results.

Cropped-Delta Wing

A cropped-delta wing having an aspect ratio of 0.87, a leading-edge sweep of 63 degrees and a taper ratio of 0.4 is analyzed with the free stream at a Mach number of 0.3 and the wing at an angle of attack of 19.95 degrees. All edges of this wing are sharp; therefore, the point of flow separation is unambiguously fixed at these edges. The results presented here illustrate the effect of varying the coefficients of the dissipation terms as well as the grid density on the solution.

Two O-O grids, one having 24,576 (64x32x12) cells and the other with 110,592 (96x48x24) cells, are used. For the coarse grid, the wing is defined by 64 cells in the chordwise direction (32 each on the upper and

lower surfaces) and 12 cells in the spanwise direction between the root and the tip. The corresponding numbers for the fine grid are 96 (48 each on the upper and lower surfaces) and 24. The grids were generated using the Boundary Integral Grid (BIG) generation technique [18]. A typical distribution of cells for the fine grid is shown in Figure 3.

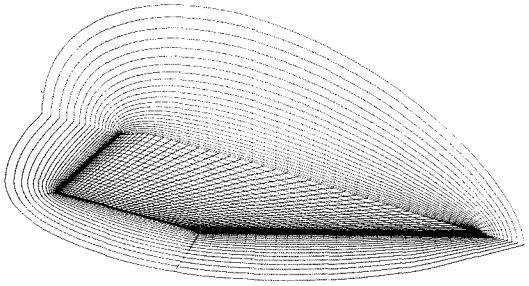

Figure 3. Oblique View of 96x48x24 O-O Grid about Cropped Delta Wing

The effect of varying VIS-2 and VIS-4 on the average residual for the coarse-grid analysis is shown in Figure 4(a). The average residual refers to the root-mean-square value of the error in the mass-conservation equation. The corresponding convergence histories for the lift coefficient are shown in Figure 4(b). The dramatic impact of varying the value of VIS-4 is quite clear from these results. It should be noted that varying the values of VIS-2, while holding constant the value of VIS-4, leads to rather small changes in the aerodynamic parameters as well as the surface pressure distributions, as shown in Figure 5. Of course, larger values of VIS-2 tend to diffuse the vortex.

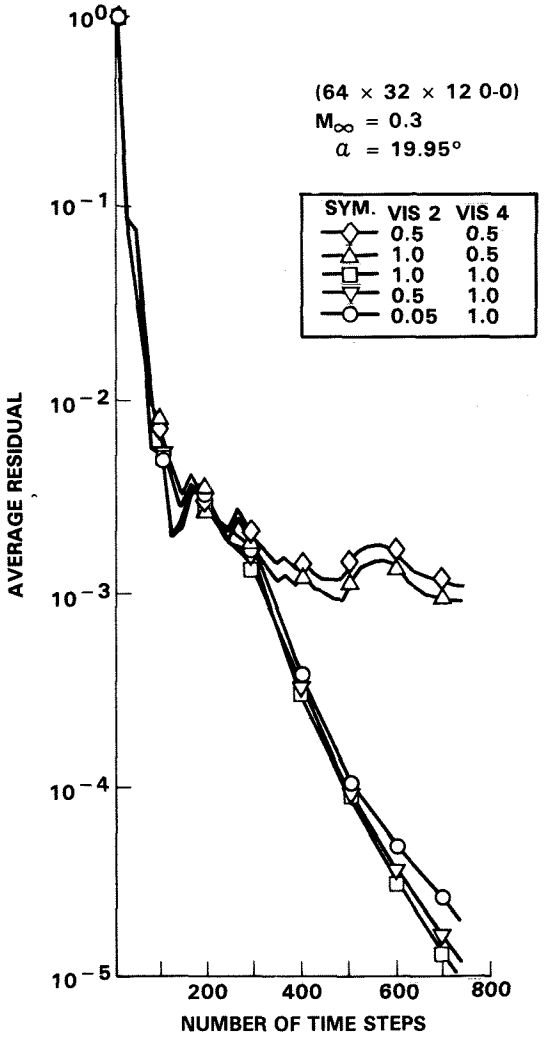

Figure 4(a). Effect of Numerical Dissipation on Convergence Rate for Cropped Delta Wing

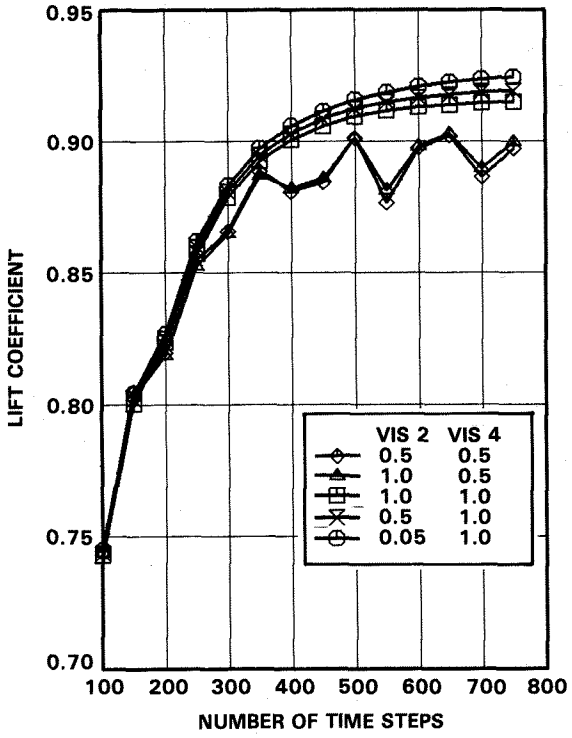

Figure 4(b). Effect of Numerical Dissipation on Lift Convergence for Cropped Delta Wing

To obtain the same level of convergence for the fine grid analysis as for the coarse grid, the value of VIS-4 had to be increased to 3.0 while keeping VIS-2 fixed at 0.05. This reflects the effect of reduced cell size which decreases the magnitude of the fourth-difference terms. Computed cross-plane surface pressure distributions for the two grids are compared in Figure 6. Increasing the number of cells results in a better resolution of the flow field, especially in the central sections of the wing. However, the differences are minimal for all practical purposes.

In Figure 7, the cross-plane surface pressure distributions computed using the TEAM code are correlated with the predictions of the FVS code, conical theory, and measured data of Luckring, et al. [6]. In general, the TEAM results are in good agreement with those of the FVS code. Since the latter has no numerical viscosity, the present

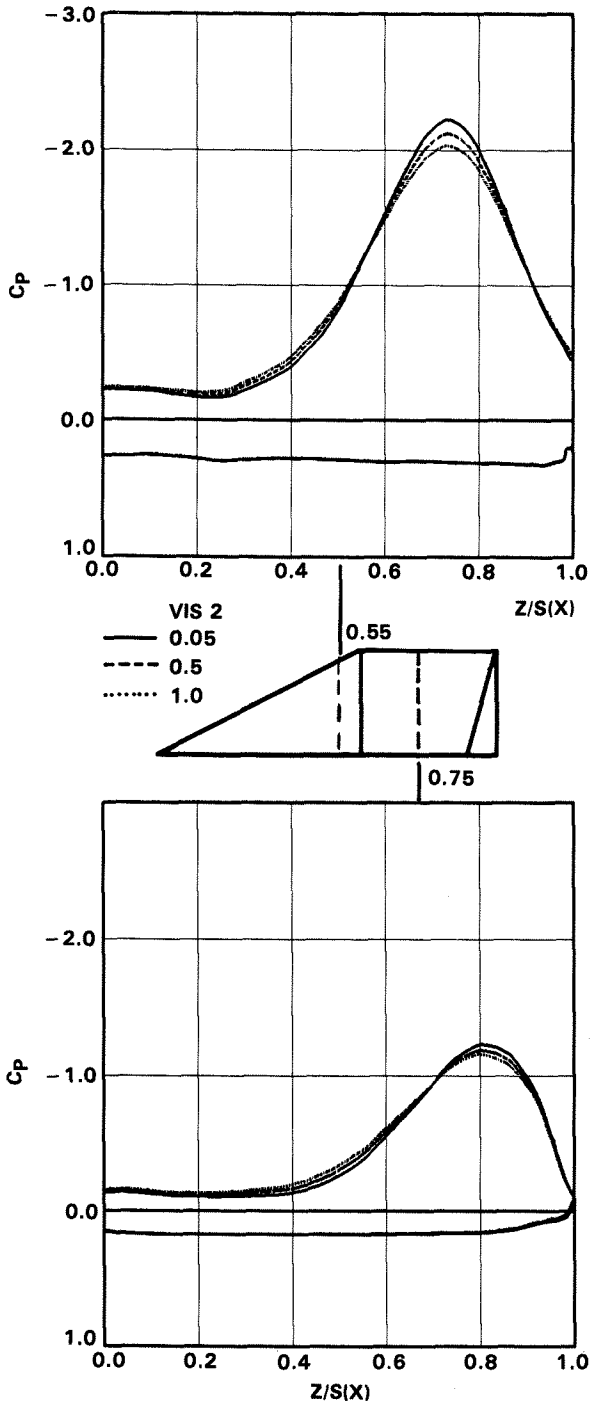

Figure 5. Effect of VIS-2 Variation on Surface Pressure Distribution for Cropped Delta Wing

correlations confirm that TEAM's artificial viscosity has not significantly corrupted the global features of this inviscid solution to the Euler equations. Both of these codes fail to capture the secondary vortices resulting from boundary-layer separation, the presence of which is strongly suggested by the experimental data. This absence of secondary vortices in the computed results is primarily responsible for the lateral shift between the computed and the measured pressure peaks. The computed cross-plane velocity vector plots presented in Figure 8 show the location of the free vortex relative to the wing.

The correlations for this wing demonstrate the ability of the TEAM code to simulate global features of inviscid leading-edge vortex flows at high angle of attack and low Mach numbers. It must be noted that the free vortices are automatically captured by the TEAM code, whereas the FVS code requires their explicit modeling.

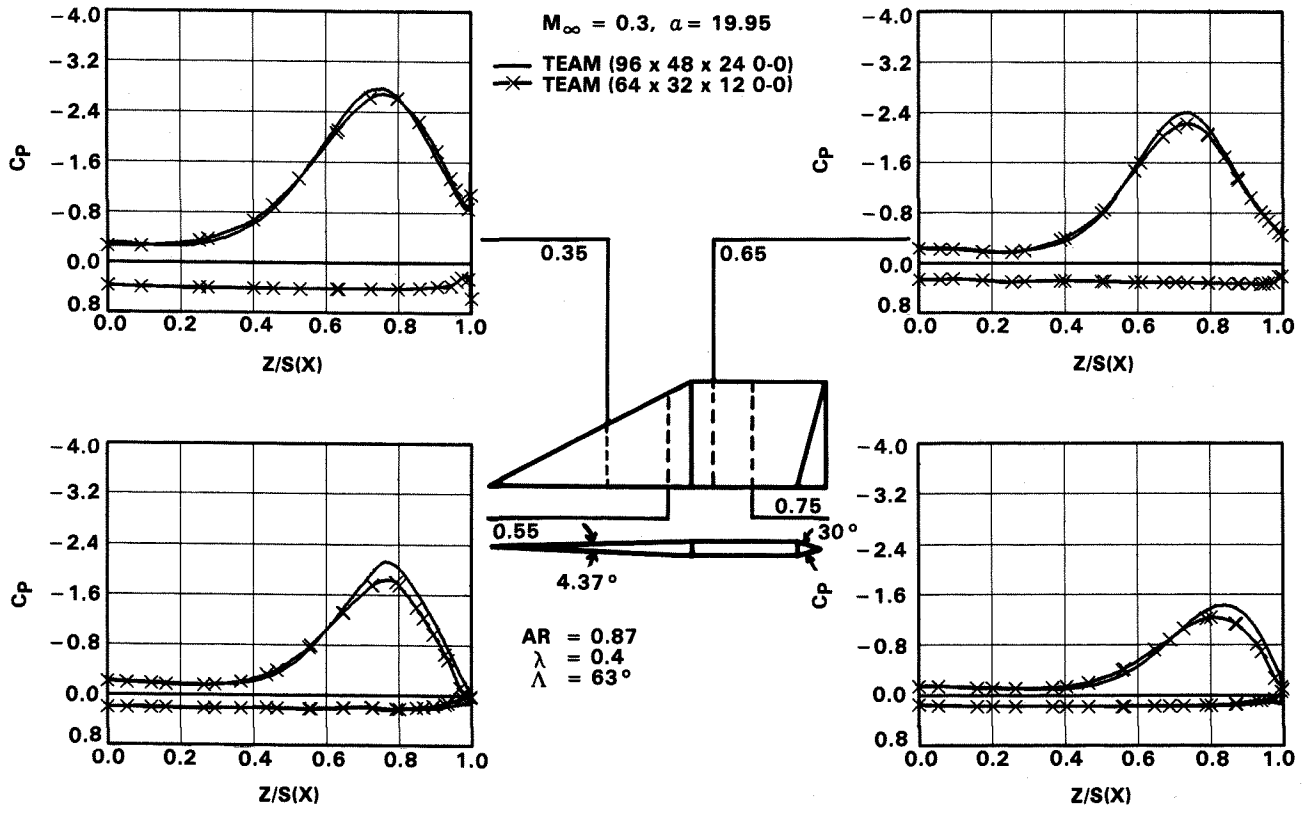

Figure 6. Effect of Grid Density on Surface Pressure Distribution for Cropped Delta Wing

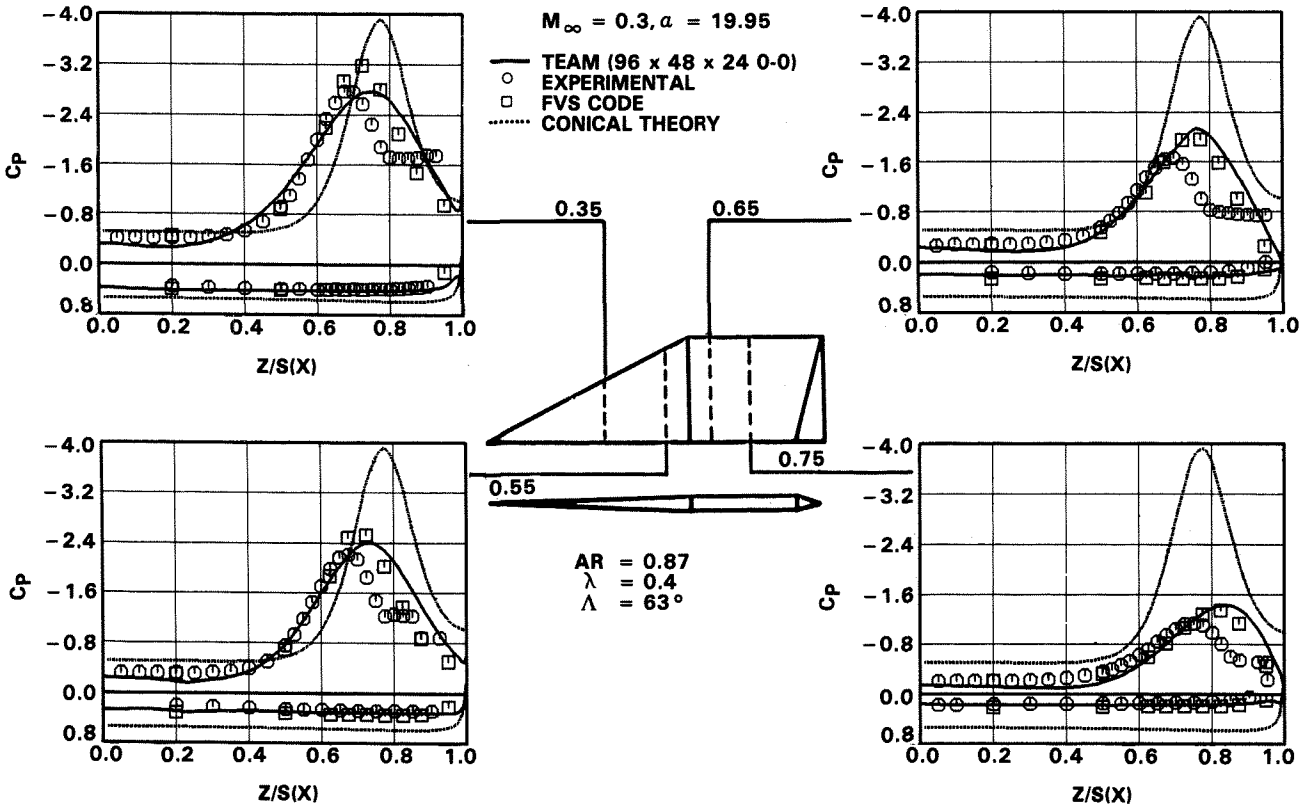

Figure 7. Cross-plane Surface Pressure Correlations for Cropped Delta Wing

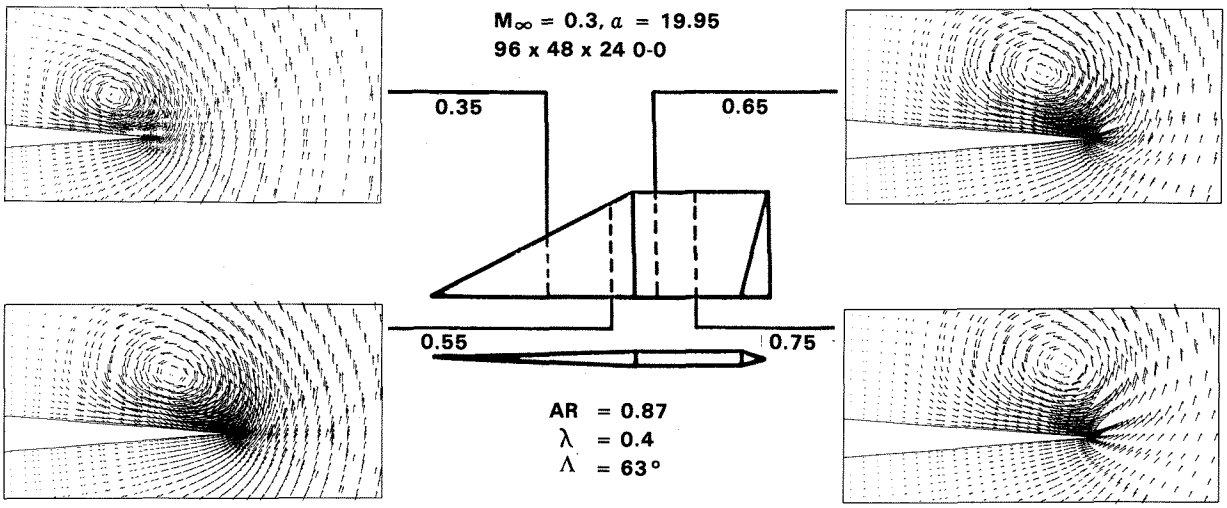

Figure 8. TEAM Prediction of Cross-plane Velocity Field for Cropped Delta Wing

Arrow Wing

An arrow wing with an aspect ratio of 1.4, a leading-edge sweep of 71.2 degrees, and a taper ratio of 0.1 is the second case considered here. The wing is composed of airfoil sections that are approximately three percent thick. Computations were carried out using two O-O grids, one having 24,320 (76x20x16) cells and the other with 109,440 (96x38x30) cells. The grids were generated using the BIG code. A partial view of the denser grid is shown in Figure 9(a). Results are presented for both round and sharp leading edges, the corresponding grids of which are shown in Figures 9(b) and 9(c).

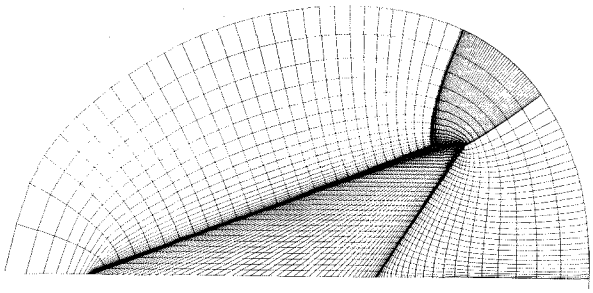

Figure 9(a). Planform View of 96x38x30 O-O Grid about Arrow Wing

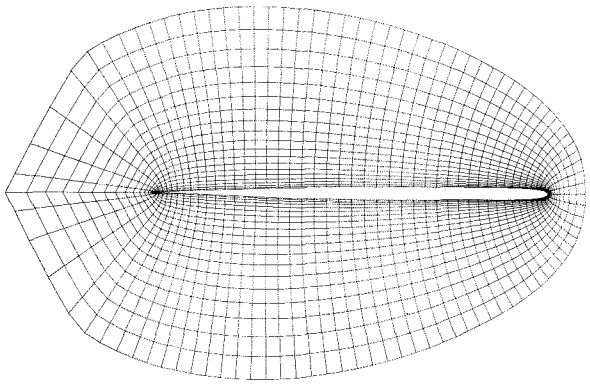

Figure 9(b). Typical Chordwise Grid Section about Round Leading-edge Arrow Wing

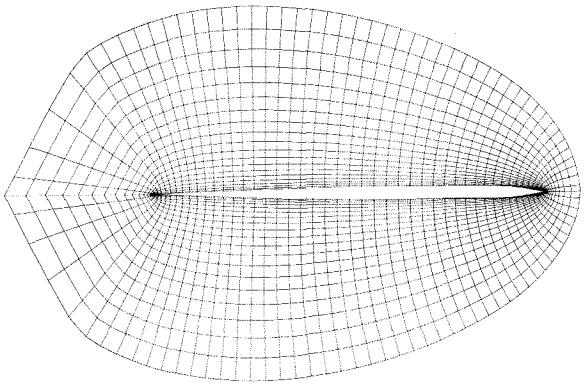

Figure 9(c). Typical Chordwise Grid Section about Sharp Leading-edge Arrow Wing

In Figure 10, computed aerodynamic parameters for the round leading-edge wing using the denser grid at a free-stream Mach number of 0.85 and at angles of attack of 4.0, 7.9, and 15.8 degrees are correlated with experimental data [19]. The overall agreement is satisfactory. It must be noted that the wind-tunnel test was for a wing-body configuration, and the data presented in this figure correspond to the integrated values using measured pressures on the wing.

The effect of grid density on the solution for this wing is illustrated by the correlations of the computed pressure distributions with measured values presented next. For the round leading-edge wing at 15.8-degree angle-of-attack, the correlations at four cross-plane stations are shown in Figure 11(a). Similar correlations for the sharp leading-edge wing are presented in Figure 11(b). The surface-pressure levels and the vortex locations show considerable dependence on the grid density. This reflects the inadequacy of the coarse grid to model a flow that is quite complex due to the presence of shocks in addition to the free vortices. In contrast, the subsonic-flow results of the sharp-edged cropped-delta wing exhibit much less sensitivity to the grid density.

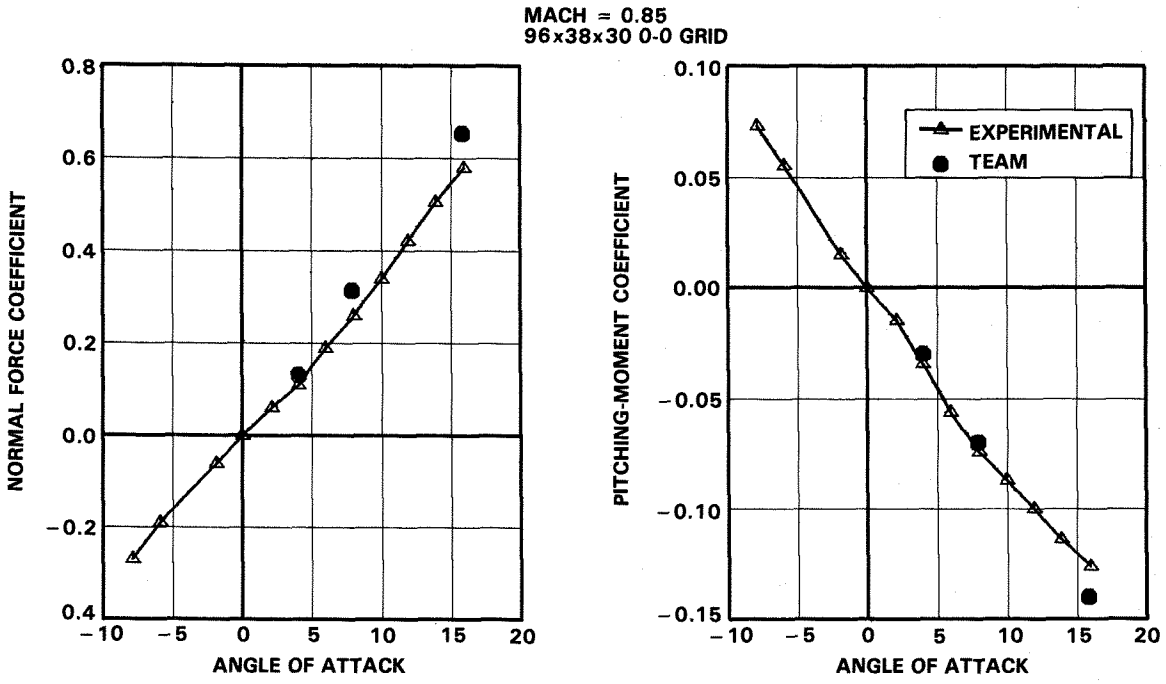

Figure 10. Correlation of Computed and Measured Aerodynamic Parameters for Round Leading-edge Arrow Wing

The next set of results shows the effect of leading-edge shape. The computed cross-plane pressure distributions for the round and sharp leading-edge wings are compared to each other for the coarse-grid analysis in Figure 12(a) and for the fine grid in Figure 12(b). It is interesting to note that the effect of the leading-edge shape is rather localized to the leading-edge region for both grids. On each of the grids, global features of the flow are essentially the same. The experimental data also show minimal effect of the leading-edge shape on the flow field.

The results presented here demonstrate TEAM's ability to model the free vortex flow at transonic Mach numbers. However, the solutions exhibit considerable dependence on grid density. Additional studies using denser grids are required to validate the code. Even though the effect of leading-edge shape on the computed results is minimal, further study is required in light of recent investigations [20,21] where the results for round-edge configurations are found to be sensitive to variations in grid density and numerical dissipation.

Strake-Wing-Body

The last set of results presented in this paper is for a strake-wing-body configuration [22], shown schematically in Figure 13. The wing has biconvex airfoils, and both the strake and wing have sharp leading edges. A 96x32x32 C-H grid (98,304 cells) generated using the PACMAPS (PArabolic and Conformal MAPping with Shearing) technique [23] was used. An oblique view of the grid is shown in Figure 14. The fuselage is treated as a bump on the plane of symmetry. There are seventeen C curves between the strake-wing/fuselage juncture and the fuselage crown. The strake-wing (and wing itself for wing-body analysis) is defined by 60 cells (30 each on the upper and lower surfaces) in the chordwise direction and 22 cells in the spanwise direction between the root and the tip sections.

Values of computed lift coefficient for strake-on configuration at a free-stream Mach number of 0.5 are compared with experimental data [22] in Figure 15. Two observations deserve mention here: (1) A steady-state solution could not be obtained for the 30-degree angle-of-attack case, whereas the average residual decreased by four to five orders of magnitude for other cases, as shown in Figure 16. Different values of numerical dissipation coefficients did not affect this lack of convergence. (2) There is excellent agreement between the computed and measured values at lower angles of attack but not at higher ones.

As regards the first observation, a closer examination of the flow field revealed the probable cause of this unsteadiness to be a "vortex burst." It is illustrated in Figure 17 by the velocity vectors at three cross-plane stations at three different stages in the solution process. Since pseudo-time stepping was used, the unconverged solution is not physically meaningful except perhaps in a qualitative sense. Similar behavior has been observed in the computational simulation of a cropped-delta wing [24] and a cranked-delta wing [25,26]. Time-accurate calculation suggests itself as an alternative for

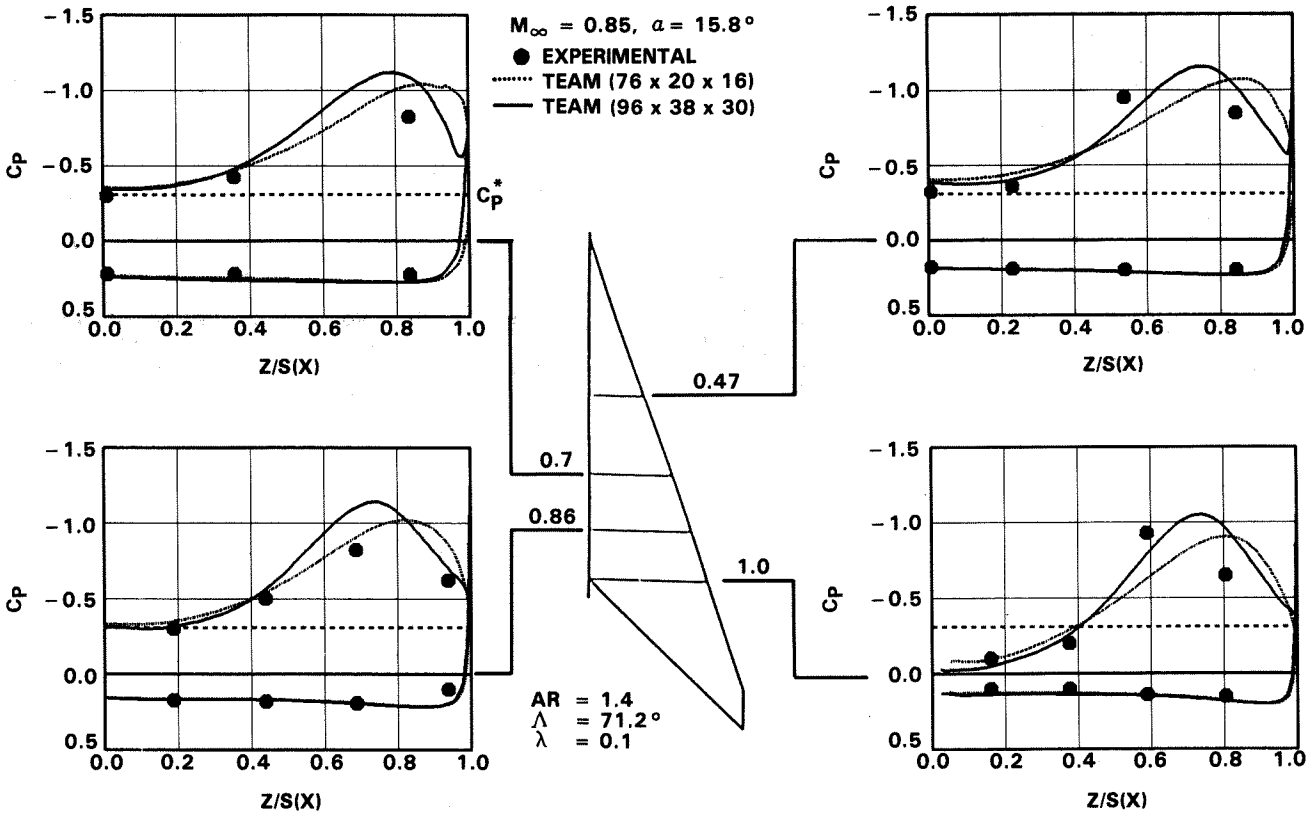

Figure 11(a). Cross-plane Surface Pressure Correlation for Arrow Wing with Round Leading Edge

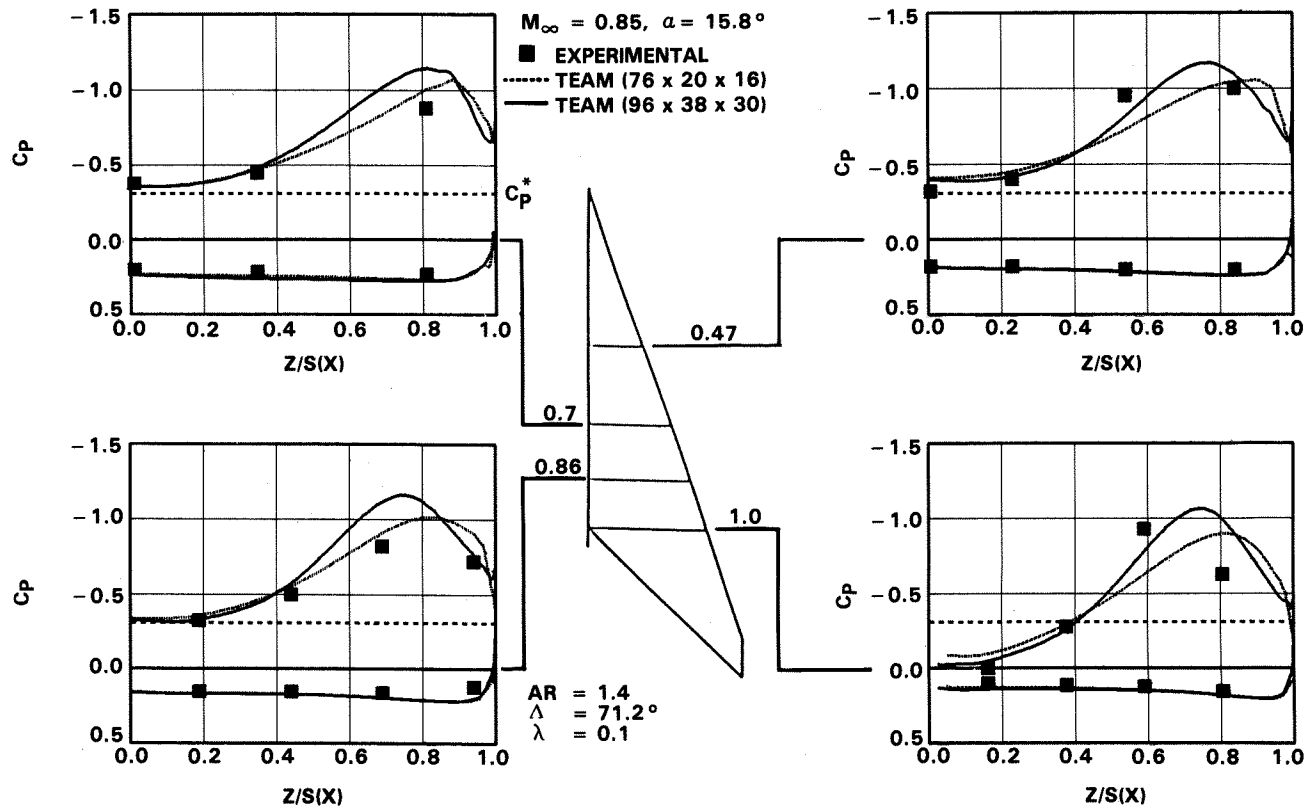

Figure 11(b). Cross-plane Surface Pressure Correlation for Arrow Wing with Sharp Leading Edge

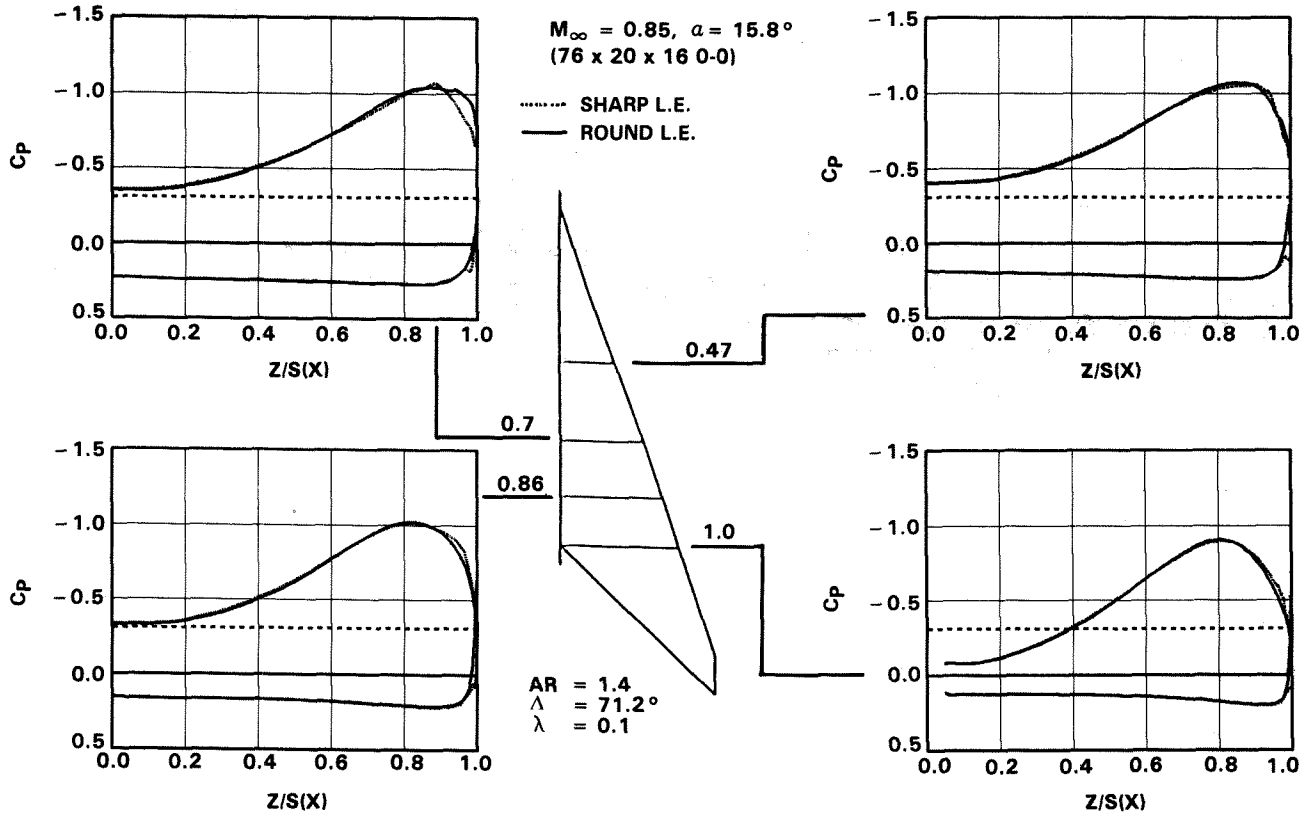

Figure 12(a). Effect of Leading-edge Shape on Computed Cross-plane Surface Pressures for Coarse Grid Analysis

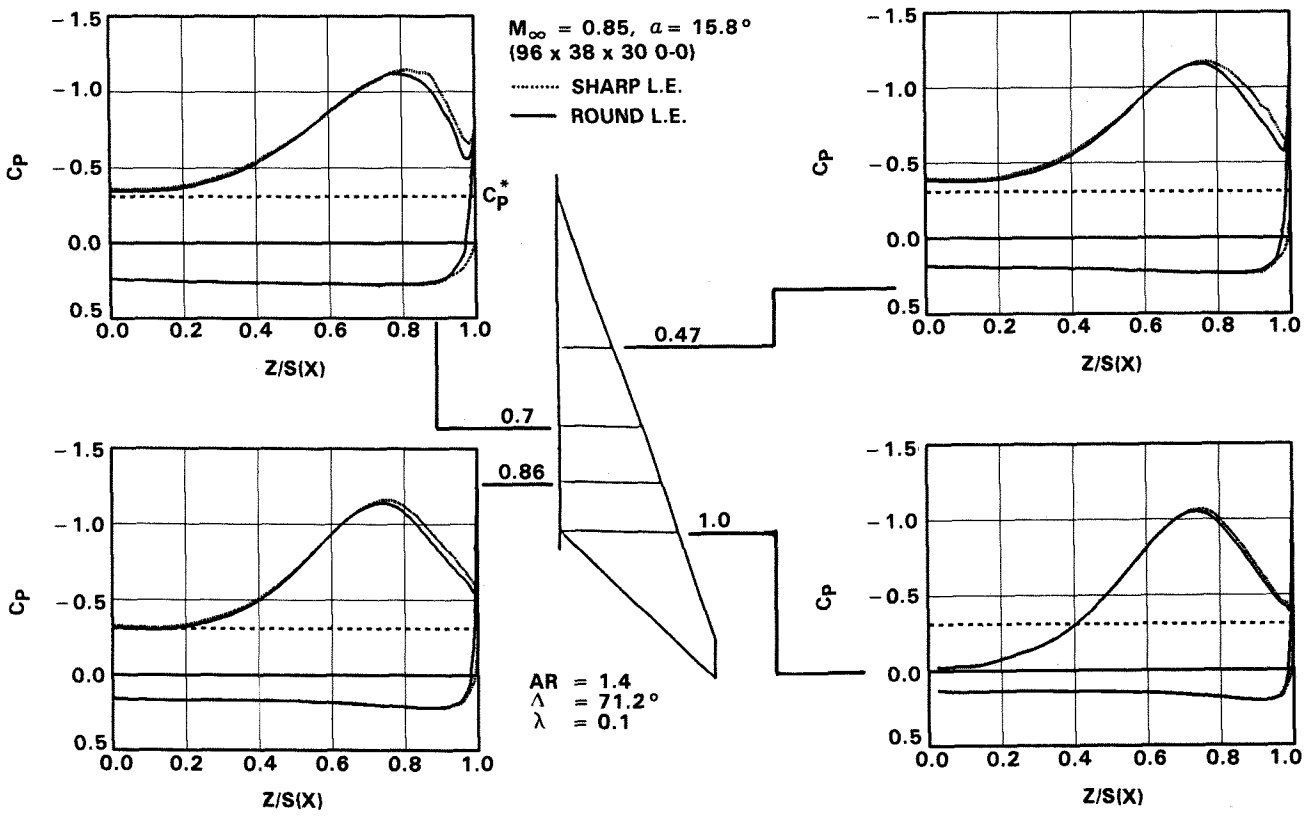

Figure 12(b). Effect of Leading-edge Shape on Computed Cross-plane Surface Pressures for Fine Grid Analysis

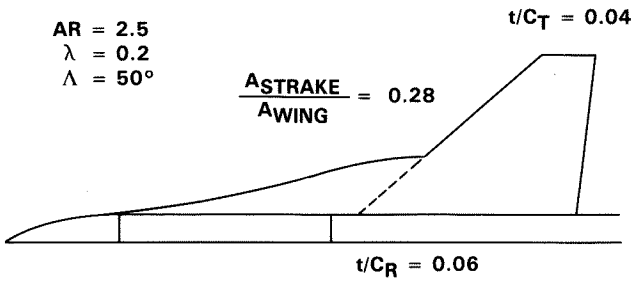

Figure 13. Plan View of Strake-Wing-Body Configuration

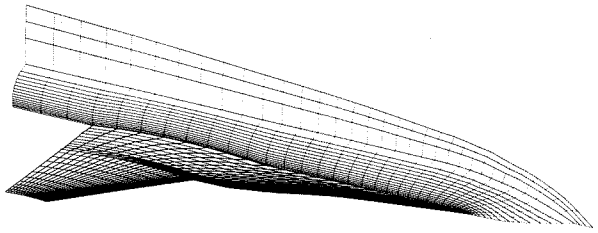

Figure 14. Oblique View of C-H Grid about Strake-Wing-Body Configuration

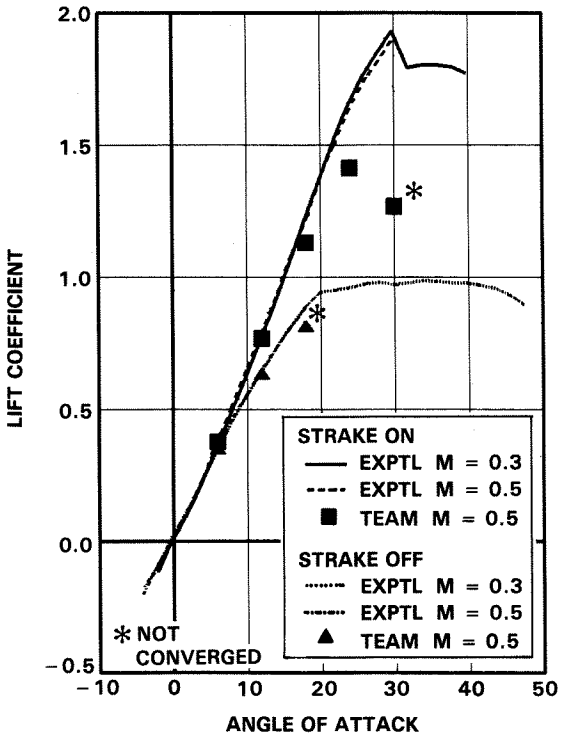

Figure 15. Lift-Coefficient Correlation for Strake-on and Strake-off Configurations

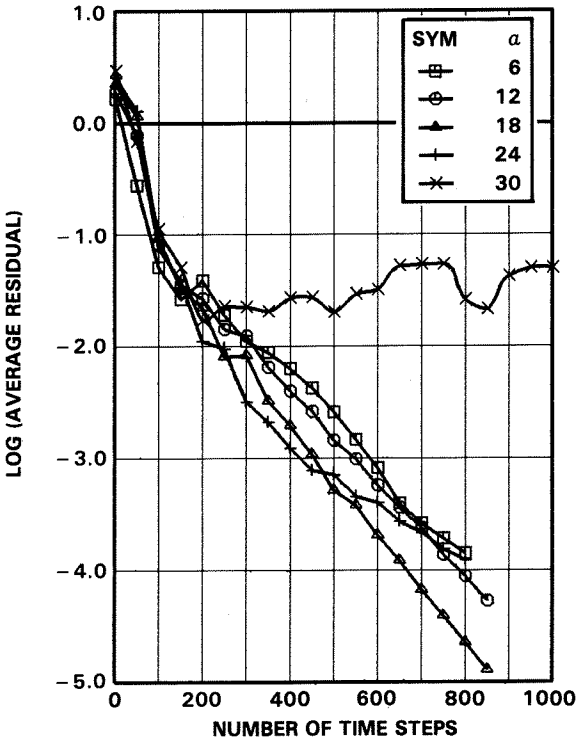

Figure 16. Convergence History for Strake-on Configuration

further analysis but the associated prohibitive cost is the major obstacle at present. It is nevertheless interesting to note that this angle of attack falls in the region where the experimental data exhibit the effects of vortex burst.

There are at least two possible sources of discrepancies between converged solutions at higher angles of attack and measurements as shown in Figure 15. The first involves the vortices generated by the separation of boundary layer on the forebody at angles of attack higher than 15 degrees. Their presence is confirmed by oil-flow patterns shown in Reference 27. These vortices are not automatically captured by the inviscid Euler code. The second is the relatively sparse cell distribution away from the surface. With increasing angle of attack, the vortices move farther away from the strake-wing surface where they cannot be adequately resolved, due to the coarseness of the grid. Further analysis of this factor is continuing at the time of writing.

Correlation between the computed and measured values for strake-off configuration is also shown in Figure 15. For this case, a steady-state solution could not be obtained for the 18-degree angle-of-attack case. The cross-plane velocity vectors presented in Figure 18 clearly illustrate the source of this unsteadiness as a vortex instability over the aft part of the wing. The stabilizing effect of the strake is also demonstrated by these correlations.

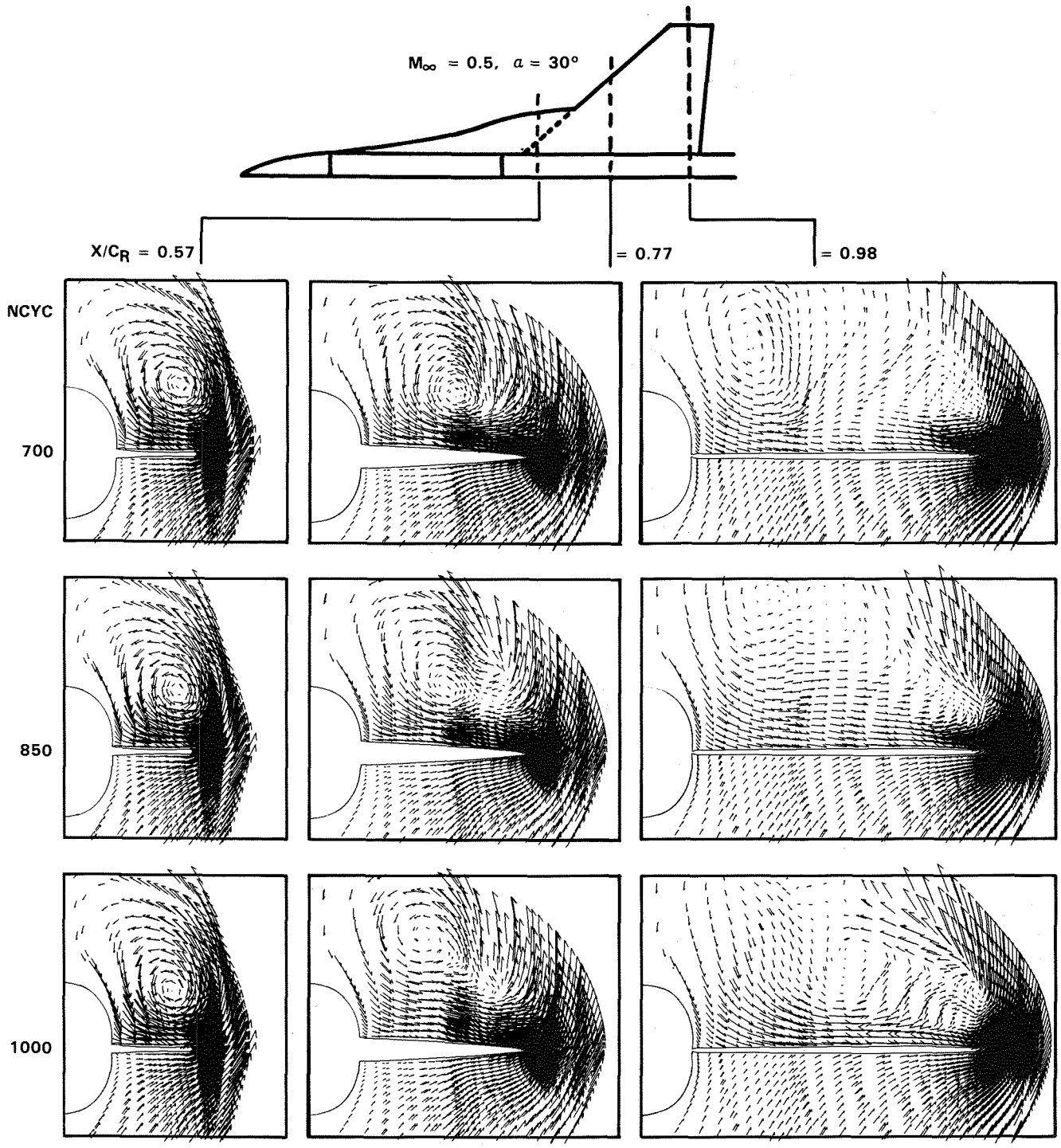

Figure 17. Local Vortex Instability for Strake-on Configuration

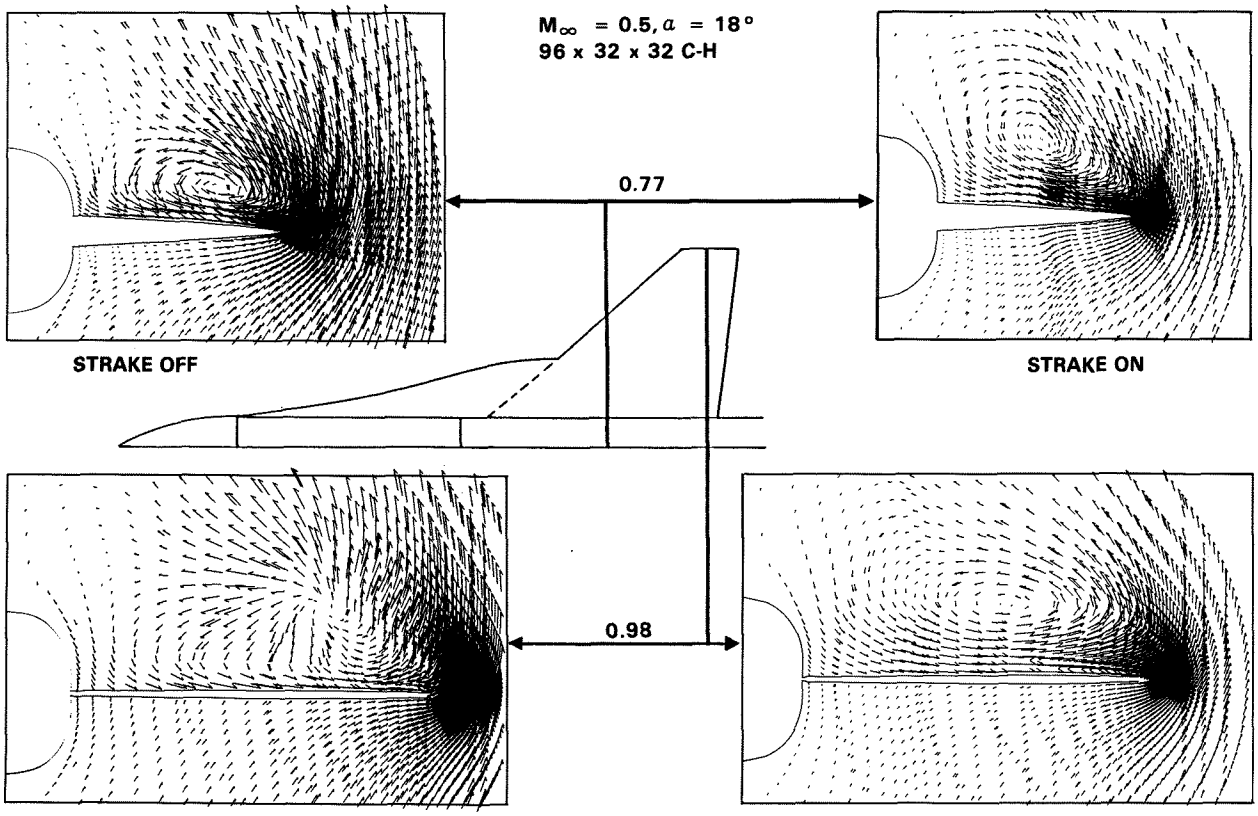

Figure 18. Stabilizing Effect of Strake on Wing-Body Flow Field

Vorticity and Numerical Dissipation

The appearance of vorticity in the steady-state solutions of the Euler equations presented here may be puzzling at first glance, since the differential equations are inviscid. However, one possible source of vorticity is contained in Crocco's theorem [28] which relates gradients of entropy, or total pressure, to gradients of vorticity for inviscid compressible flows. For computed flows containing captured shocks of variable strength, the shocks provide an obvious source of entropy gradients. Of course, the explicitly added numerical dissipation terms are crucial for capturing these shocks. Even for flows without shocks, the numerical dissipation can produce significant total pressure losses (or entropy gradients) in certain regions containing large flow gradients, e.g., near stagnation points. Inaccuracies related to the numerical implementation of the no-normal-flow boundary condition near sharp edges and regions of large curvature can further increase these losses.

Based on the results presented in this paper and other investigations by the authors, it may be concluded that generation of vortices about sharp-edged wings due to the total pressure losses is quite insensitive to the actual magnitude of the numerical dissipation, **as long as there is some**. It is not, however, very surprising, considering the observed Reynolds-number independence of a large class of leading-edge vortex flows for slender wings with sharp edges. Other recent investigations [21,26] have led to similar observations. Interpretation of separated-flow results for wings with rounded edges requires more caution. The total losses due to numerical dissipation depend upon grid density, user-specified coefficients, and flow gradients [21]. Results for the arrow wing presented above and similar results of Hitzel and Schmidt [11] suggest that the Euler solutions may provide meaningful data as long as the radius of curvature is relatively small. Further validation is required to provide useful guidelines to the designers.

Concluding Remarks

The correlations shown in this paper illustrate the capability of the TEAM code to capture vortices resulting from flow separation along the leading edges and side edges of swept, slender wings at moderate-to-high angles of attack. Unlike the procedures based on velocity potential, such as the free-vortex-sheet technique, it is not required to explicitly model the vortices. They appear automatically wherever the flow requires them. In addition, the same code can be used for analysis throughout the entire flight regime.

Based on the experience to date, the following observations related to the effect of numerical dissipation and grid density may be made:

- A larger amount of fourth-order dissipation may be required to obtain converged solutions when using finer grids. The results presented here and in other numerical experiments suggest that the effect of this dissipation on the accuracy of the solution is insignificant, as long as it stays small compared to the convective terms.

- Input values for the coefficient of the second-order dissipation terms should be small so that the regions of high gradients are properly captured but not unduly diffused.

- Fine tuning of the dissipation coefficients is not required to obtain results of engineering accuracy. For most cases, acceptable results are obtained for sets of coefficients differing by factors of two to three.

- Global features of computed free-vortex flows about sharp-edge wings are relatively insensitive to grid densities for subsonic flows. Of course, the flow field is better resolved on finer grids. The same is not necessarily true for wings with round edges.

- For certain flow configurations, the pseudo-time marching Euler solutions do not reach a steady state because the free vortices exhibit local instabilities. This issue requires further investigation.

Use of Euler codes appears to be an attractive alternative to using the Navier-Stokes codes which require greater computational resources and suffer from empiricism of turbulence modeling. This is especially true for flows that are practically Reynolds number-independent and whose primary features are not significantly altered by the vortices generated by separation of the boundary layer along smooth surfaces. With ongoing validation, the present approach promises to result in an effective method for simulating vortex-dominated high-angle-of-attack flows for engineering applications.

Acknowledgment

This investigation is entirely supported by Lockheed-California Company's Independent Research and Development program. The development of the TEAM code used in this study is partially funded by a U. S. Air Force contract. The support and encouragement of Luis Miranda, Manager, Computational & Advanced Aerodynamics Department, is gratefully acknowledged. Thanks are due to Dr. J. M. Luckring of NASA-Langley Research Center for supplying tabulated data for the cropped-delta wing.

References

1. Lamar, J.E., "Extension of Leading-Edge-Suction Analogy to Wings with Separated Flow Around the Side Edges at Subsonic Speeds," NASA TR R-428, October 1974.

2. Lamar, J.E. and Gloss, B.B., "Subsonic Aerodynamic Characteristics of Interacting Lifting Surfaces with Separated Flow Around Sharp Edges Predicted by a Vortex-Lattice Method," NASA TN D-7921, September 1975.

3. Lan, C.E. and Chang, Jen-Fu, "Calculation of Vortex Lift Effect for Cambered Wings by Suction Analogy," NASA CR 3449, July 1981.

4. Mehrotra, S.C. and Lan, C.E., "A Theoretical Investigation of the Aerodynamics of Low-Aspect-Ratio Wings with Partial Leading-Edge Separation," NASA CR-145304, 1978.

5. Johnson, F.T., Lu, P., Tinoco, E.N., and Epton, M.A., "An Improved Panel Method for the Solution of Three-dimensional Leading-edge Vortex Flows," NASA CR-3273, July 1980.

6. Luckring, J.M., Schoonover, W.E., and Frink, N.T., "Recent Advances in Applying Free Vortex Sheet Theory for the Estimation of Vortex Flow Aerodynamics," AIAA 82-0095, 20th Aerospace Sciences Meeting, Orlando, Florida, January 11-14, 1982.

7. Polhamus, E.C., "A Concept of the Vortex Lift of Sharp Edge Delta Wings Based on a Leading-Edge-Suction Analogy," NASA TN D-3767, 1966.

8. Fujii, K. and Kutler, P., "Numerical Simulation of the Leading-Edge Separation Vortex for a Wing and Strake-Wing Configuration," AIAA Paper 83-1908-CP, 6th Computational Fluid Dynamics Conference, Danvers, Massachusetts, July 13-15, 1983.

9. Jameson, A., Schmidt, W., and Turkel, E., "Numerical Solutions of the Euler Equations by Finite Volume Methods Using Runge-Kutta Time-Stepping Schemes," AIAA Paper 81-1259, 14th Fluid and Plasma Dynamics Conference, Palo Alto, California, June 23-25, 1981.

10. Rizzi, A., "Damped Euler Equation Method to Compute Transonic Flow Around Wing-Body Combinations," AIAA Journal, Vol. 20, No. 10, October 1982, pp. 1321-1328.

11. Hitzel, S.M. and Schmidt, W., "Slender Wings with Leading-Edge Vortex Separation: A Challenge for Panel Methods and Euler Solvers," AIAA Journal of Aircraft, Vol. 21, No. 10, October 1984, pp. 751-759.

12. Raj, P. and Sikora, J.S., "Free-Vortex Flows: Recent Encounters with an Euler Code," AIAA Paper 84-0135, 22nd Aerospace Sciences Meeting, Reno, Nevada, January 9-12, 1984.

13. Rizzi, A., "Computer Simulation of Nonpotential Flows Around Wings," Aeronautical Journal, June/July 1984, pp. 238-248.

14. Raj, P., "Computational Simulation of Free-Vortex Flows Using An Euler Code," ICAS-84-1.3.1, 14th Congress of the International Council of the Aeronautical Sciences, Toulouse, France, September 9-14, 1984.

15. Rizzi, A. and Eriksson, L.E., "Computation of Inviscid Incompressible Flow With Rotation," Journal of Fluid Mechanics, Vol. 153, 1985, pp. 275-312.

16. Jameson, A. and Baker, T.J., "Solution of the Euler Equations for Complex Configurations," AIAA Paper 83-1929-CP, 6th Computational Fluid Dynamics Conference, Danvers, Massachusetts, July 13-15, 1983.

17. Agarwal, R.K. and Deese, J.E., "Transonic Wing-Body Calculations Using Euler Equations," AIAA Paper 83-0501, 21st Aerospace Sciences Meeting, Reno, Nevada, January 10-13, 1983.

18. Sikora, J.S. and Miranda, L.R., "Boundary Integral Grid Generation Technique," AIAA Paper 85-4088, 3rd Applied Aerodynamics Conference, Colorado Springs, Colorado, October 14-16, 1985.

19. Manro, M.E., Manning, K.J.R., Hallstaff, T.H., and Rogers, J.T., "Transonic Pressure Measurements and Comparison of Theory to Experiment for an Arrow-Wing Configuration," NASA CR-2610, August 1976.

20. Newsome, R.W., "Euler and Navier-Stokes Solutions for Flow Over a Conical Delta Wing," AIAA Journal, Vol. 24, No. 4, April 1986, pp. 552-561.

21. Kandil, O.A. and Chaug, A., "Numerical Dissipation Effect in Finite-Volume Euler Solutions for Conical Vortex-Dominated Flows," ICCM86-K.8, International Conference on Computational Mechanics, Tokyo, Japan, May 25-29, 1986.

22. Luckring, J.M., "Subsonic Longitudinal and Lateral Aerodynamic Characteristics for a Systematic Series of Strake-Wing Configurations," NASA Technical Memorandum 78642, February 1979.

23. Raj, P., "PACMAPS: A Three-dimensional Grid Generation Method, Version 1.0," LR 30811, Lockheed-California Company, October 1984.

24. Raj, P. and Long, L.N., "An Euler Aerodynamic Method for Leading-Edge Vortex Flow Simulation," Vortex Flow Aerodynamics Conference, NASA-Langley Research Center, October 8-10, 1985.

25. Rizzi, A. and Purcell, C.J., "Numerical Experiment with Inviscid Vortex-Stretched Flow Around a Cranked Delta Wing: Subsonic Speed," AIAA Paper 85-4080, 3rd Applied Aerodynamics Conference, Colorado Springs, Colorado, October 14-16, 1985.

26. Murman, E.M. and Rizzi, A., "Applications of Euler Equations to Sharp Edge Delta Wings With Leading Edge Vortices," AGARD Symposium on Application of Computational Fluid Dynamics in Aeronautics, Aix-en-Provence, France, April 7-10, 1986.

27. Luckring, J.M., "Flow Visualization Studies of a General Research Fighter Model Employing a Strake-Wing Concept at Subsonic Speeds," NASA Technical Memorandum 80057, August 1979.

28. Liepmann, H. W. and Roshko, A., "Elements of Gasdynamics," John Wiley & Sons, Inc., 1957, p. 193.